N87-28791

TDA Progress Report 42-90 April–June 1987

DSS 43 64-Meter Antenna S- and X-Band Efficiency and System Noise Temperature Calibrations, January 1987

S. D. Slobin
Radio Frequency and Microwave Subsystems Section

The DSN 64-m antenna in Australia (DSS 43) has been calibrated prior to its upgrading to a 70-m High Efficiency configuration in preparation for the Voyager Neptune encounter in August 1989. The S-band (2285-MHz) and X-band (8420-MHz) antenna area efficiency and system noise temperature calibrations were carried out during December 1986 and January 1987 to establish a baseline system performance for this station. This article is the second in a series documenting 64-m and High Efficiency 70-m and 34-m antenna performance improvements for the NASA/JPL Deep Space Network. The agreement between theory and measurement is excellent.

I. Introduction

This article is the second in a series documenting the performance of the 64-/70-m antennas in the pre-70-m (1986/87) and post-70-m (1987/88) configurations, as well as the performance of the 34-m High Efficiency antennas. The article on the 64-m station in Spain (DSS 63) is presented elsewhere in this issue [1]. Much of the general description of the antenna calibration methodology and data reduction techniques is given in that reference. The descriptions given in this article will therefore not be as detailed.

Antenna calibration measurements were taken during the months December 1986 and January 1987 on five separate days. Because of weather conditions documented in the reports as "storm cloud," "mid-level cloud-like thick fog," and "shower-type cloud," data from days 1986/339 and 349 and 1987/012 were not used. The remaining two days, 1987/018 and 020, appear to have had good weather, and those days provided the data for the antenna calibration. The radio sources observed were 3C274, 3C218, and 0521–365. The sources 3C274 and 3C218 are regarded as DSN standard calibrators, but it was found that both 3C218 and 0521–365 needed adjustments of their accepted values of 100-percent area-efficiency antenna temperature in order to obtain agreement with the 3C274 measurements. The largest correction was 14 percent, applied to source 0521–365 at X-band. A correction of this size undoubtedly arises from the use of an incorrect value of flux density in the antenna gain analysis (AGA) data reduction program. All other corrections were in the range of 1 to 3 percent. This aspect of the calibration will be discussed later. For reference, the 100-percent area-efficient gain of a 64-m-diameter antenna at S-band (2285 MHz) is 63.71 dBi. At X-band (8420 MHz), it is 75.04 dBi. A comprehensive description of the adjustments made to the theoretical X-band gain values to predict actual antenna performance is given in [1].

Efficiency and noise temperature curves are presented both with and without the atmospheric effects included. The measurements, of course, were made with the antenna immersed in the earth's atmosphere. At a 10-deg elevation angle, the antenna looks through nearly six zenith-equivalent atmospheres, and radio source noise temperature contributions are attenuated by nearly 0.25 dB at X-band. The effective efficiency [2] is thus somewhat lower than the real antenna efficiency. This atmospheric effect must be removed to determine the true inherent quality of the antenna itself. It is recommended that for all telecommunications link analyses, the atmosphere-free antenna parameters be used. In that way, any known or postulated atmospheric effect (noise temperature and attenuation) can be added fully and directly into the link calculations.

II. Antenna Area Efficiency

Figures 1 and 2 show the S-band antenna efficiencies both with and without the atmospheric attenuation effect, respectively. It was found when looking at the raw AGA data (cf. [1]) that there was some inconsistency in comparisons of antenna efficiency as determined by two different radio sources at the same elevation angle. For the complete set of data, it was found at S-band that source 3C218 yielded efficiencies which were high compared to those determined by source 3C274. Conversely, source 0521-365 yielded efficiencies which were too low compared to those determined by source 3C274. At X-band, both sources yielded efficiencies that were too high. Since it is unknown at the present time where the uncertainty lies (either in flux density or source size correction factor), the efficiency correction is adjusted, equivalently, by modifying the value of 100-percent area-efficient antenna temperature (M. J. Klein, personal communication and [2]). Included in this value are the unknown source characteristics, to be more accurately determined at a later date. Thus, if efficiency values are measured to be too high (by some determination), then the *expected* noise temperature increase from that radio source is modified *upward*. It must be remembered that this adjustment is made relative to a well-known, strong radio source, 3C274, which is one of the DSN standard calibrators. Radio source 3C218 is substantially weaker than 3C274 (one-fifth as strong) and subject to larger measurement error; thus, its determination of antenna efficiency was modified in deference to the 3C274 values. This technique is valid and is commonly used. It allows antenna efficiency values to be obtained at elevation angles where no standard calibration sources can be found. Clearly, this bootstrapping technique allows interim calibrations of new radio sources for use with other antennas *at the same frequency and with the same beamwidth*. The adjustments made to the observed radio sources are listed in Table 1. These adjustments are made to the AGA-calculated efficiency values, not to the expected antenna temperature increases. They should not be regarded as a definitive DSN calibration of those radio sources.

The atmosphere adjustment is made according to the description given in [1]. The values used for S- and X-band zenith atmospheric attenuations are 0.03 and 0.04 dB, respectively.

Second-order curves were fitted to the data shown in Figs. 1 and 2. These curves are of the form

$$\text{efficiency} = a_0 + a_1\theta + a_2\theta^2$$

where

θ = elevation angle, degrees

The coefficients of this expression for the S-band efficiency curves are given in Table 2.

Similarly, Figs. 3 and 4 show the X-band efficiency determinations for the conditions with and without atmosphere. The coefficients of the efficiency expression are also given in Table 2.

A comparison of Figs. 3 and 4 of this article with the similar figures in the DSS 63 calibration report [1] will show that the X-band efficiency curves for DSS 43 are much flatter than for DSS 63. This is due to the main reflector bracing difference between the two antennas. The DSS 43 antenna had the same bracing upgrade as the DSS 63 antenna, but in the case of the DSS 63 antenna, the original braces were not removed as intended. The DSS 43 and DSS 14 (Goldstone) 64-m antennas existed in their proper configurations before the 70-m upgrade, and the subreflector focusing movement[1] needed to compensate for main reflector and quadripod deformation was optimum for that configuration. Since identical subreflector focusing was maintained for DSS 63, it is felt that this is one cause of the large efficiency fall-off, the other being the compromised bracing situation at DSS 63, which existed for a short interim period, including the July 1986 tests.

III. System Noise Temperature

Figures 5 and 6 show the S-band system noise temperatures (with and without atmospheric effect) obtained on days 1987/018 and 020. These measurements are the off-source back-

[1]JPL Software Specification Document No. DFA-5222-OP, "Antenna Mechanical Subsystem – Subreflector Controller for 64M Antennas" (internal document), Jet Propulsion Laboratory, Pasadena, Calif., March 21, 1986.

ground reference temperatures, and thus do not depend on any of the characteristics of the radio sources such as flux density or source size correction. The S-band measurements show two distinct sets of results. This is felt to be due to a possible error in calibration of the noise-adding radiometer noise diode. No weather-dependent cause of noise temperature variation appears to explain the data. Also, no information exists which might enable a choice of data sets. A closer look at the efficiency curves (Figs. 1 and 2) shows a hint of this problem at elevation angles below about 40 degrees. Again, no choice of data sets was possible, and the accuracy of these data must be regarded as somewhat compromised by a long-period varying systematic error. (This error type will be regarded as random for the sake of analysis in this article.) Fortunately, the S-band telecommunications data are generally less critical to the DSN than are X-band data, and the large S-band uncertainties will not severely compromise link performance.

Figures 7 and 8 show the X-band off-source system noise temperatures on days 1987/018 and 020, for the conditions with and without atmospheric contribution, respectively. These data are well behaved in contrast to the S-band noise temperatures, although there also may be a hint of systematic error seen in the 1-K mismatch of noise temperatures in the 55- to 60-degree elevation angle region. These data were taken 5 hours apart, and it is possible a changing noise diode contribution or a clear-air atmosphere change may have contributed to the difference. More frequent noise diode calibration (possibly several times per hour) may assist in reducing further problems in this area. Table 3 lists the fourth-order curve-fit coefficients and standard deviation of curve fit for the curves shown in Figs. 5 through 8. In addition, certain maser preamplifier information (serial number and noise temperature) is also given.

IV. Error Analysis

As stated in [1], a comprehensive error analysis of the entire antenna calibration project will be forthcoming. In the case of the DSS 43 64-m antenna calibration, the ±1 percent S-band efficiency variation and the ±2-K S-band noise temperature variation over the 10- to 30-degree elevation angle range give a clue to the size of the long-term random errors (several hours to 1 day) that may be encountered. The data taken over the 10- to 30-degree elevation angle range appear to consist of two distinct sets, one taken on each day. It is possible that on one day the noise diode contribution varied and on the other it did not. At X-band, however, the efficiency values show a spread at low elevation angles, without a corresponding spreading of the noise temperature values. It is possible then, that an error source independent of noise temperature measurement (pointing correction, for example) may have contributed to this problem. It is not possible at this time to fully resolve pointing correction errors, if any, which may exist in the data. To do this would require an extremely precise measurement of X-band antenna beam shape in the region out to 10 millidegrees from beam peak and down to 1 dB below peak antenna gain.

It should also be noted that in general there may not be an easily observed correspondence between noise temperature variation (interpreted as a random error) and antenna efficiency measurement. For example, if a 0.05-dB (1.2-percent) source of atmospheric attenuation were to obscure the observing region, one would see both an on- and off-source noise temperature increase of about 3 K, a system noise temperature increase of about 10 percent. The derived antenna efficiency would show a variation of about 0.6 efficiency-percent for a 50-percent efficient antenna. This efficiency variation might not be easily separated from other random errors, and the observer would be puzzled as to why such a large change in off-source noise temperature did not significantly affect the calculated efficiency value.

As stated in the DSS 63 calibration report [1], it is unlikely that instrumental systematic errors exceeding ±0.2 dB (±5 percent) with 3-σ confidence are present. These errors are primarily due to receiving system nonlinearities and result in a more or less constant miscalibration of the noise-adding radiometer noise diode. The determination of the linearity correction, however, is also subject to random errors. The measurable result of this is an incorrect system noise temperature determination and hence an incorrect estimate of antenna efficiency. In the AGA program, these nonlinearities are measured and analytically removed, but not perfectly. For the purpose of the error analysis done here, any long-term variability (hours to days) in noise diode contribution or linearity change are assumed to exist as random errors, and as such they are included in the standard deviation of curve fits as presented in Tables 2 and 3.

Typical random errors, as determined from curve-fit standard deviation, appear to be ±0.1 dB (3σ) for S-band efficiency and ±0.15 dB (3σ) for X-band efficiency. The radio source flux density accuracies are estimated to be ±0.3 dB and ±0.5 dB (3σ) [1] for S- and X-band, respectively. Thus, it may be stated that the absolute accuracy in the determination of antenna efficiency for the DSS 43 antenna is

S-band: ±0.4 dB (3σ)

X-band: ±0.6 dB (3σ)

The radio source flux uncertainty is the major contributor to the error in determination of antenna efficiency. Until radio

source flux density is more accurately defined, further work to reduce instrumental systematic errors will not materially change the present overall accuracy of antenna efficiency.

For noise temperature accuracy, only the systematic and random errors need be considered. For Figs. 5 and 7, the S- and X-band noise temperature curves, the curve-fit random errors are 0.4 dB and 0.2 dB (3σ), respectively. Thus, in conjunction with the systematic error of 0.2 dB, it is stated that the error in determination of system noise temperature is

S-band: ± 0.5 dB (3σ)

X-band: ± 0.3 dB (3σ)

corresponding to ± 3.1 K at S-band and ± 1.8 K at X-band, 3σ, for a nominal 25-K system noise temperature.

V. Comparison of Measured and Expected Antenna Efficiencies

In a manner entirely similar to that presented in [1], a comparison was made among the X-band antenna performance expectations as given by physical optics (PO) and geometrical theory of diffraction (GTD) programs, with modifications to the GTD curves to account for varying levels of small-scale surface irregularity due to main reflector panel manufacturing and setting tolerances, and subreflector manufacturing tolerance. The GTD program gives efficiency determination as a function of elevation angle. This varies, due primarily to gravity-induced main reflector distortion. Since the main reflector is not a perfect paraboloid away from the rigging angle (and hence has only a best-fit focus), subreflector focusing is accomplished only in a best-fit sense.

Table 4, reproduced directly from [1], shows the expected feed system losses (calculated by the PO program) and hardware losses which reduce theoretical 64-m antenna performance. A full description of the elements of this table appears in [1]. It is found that the PO and GTD analyses predict nearly identical antenna performance (within 0.1 dB at the 74.02-dBi point in Table 4). Again, it is noted in the table that the expected small-scale (Ruze) surface tolerance is 1.06 mm for a newly manufactured and very well-adjusted 64-m antenna.

Figure 9 shows a comparison of measured antenna area efficiency (without atmosphere, Fig. 4) and expected values of efficiency as given by GTD calculations of antenna gain, reduced by known or postulated hardware losses. In this figure, GTD calculations with adjustments of 0.821 dB for known loss and a Ruze loss corresponding to an rms surface error of 1.06 mm appear as the top curve, with a maximum efficiency of 0.584. The measured efficiency curve appears with a maximum value of 0.454, which is 1.09 dB lower than theoretical. This difference is explainable to a large extent by the examination of Fig. 10. Similar GTD calculations, but with additional Ruze rms surface tolerances of 1.5, 1.8, and 2.0 mm, are shown. It is seen, as in the DSS 63 case, that the acceptance of a 1.7- to 1.8-mm rms level of small-scale surface roughness gives excellent agreement with the measured curve. It should also be noted that the peak experimental efficiencies (without atmosphere) of DSS 43 and DSS 63 are virtually identical (0.454 for DSS 43 vs 0.451 for DSS 63).

The S-band holographic tests[2] carried out on this antenna in January 1985 indicate an rms surface error (for 0.4-m resolution) of 2.09 mm for a 64-m-diameter surface, and 1.74 mm for a 57-m-diameter surface, excluding the outer ring of panels. It was predicted that potential rms surface errors of 1.33 and 1.06 mm, respectively, would result after panel readjustment. Although panels were reset in August 1985, substantial improvement obviously did not result. The fact that both DSS 43 and DSS 63 show a 1.7- to 1.8-mm surface (as deduced by X-band GTD/Ruze calculations and experiment) supports the January 1985 holography measurements. The fact that the X-band efficiency measurements were made *after* the August 1985 panel reset indicates that there may exist some reflector surface irregularity (or a holography limitation) which is not allowing surface adjustment below the 1.7-mm rms level.

Holography produces a data type which optimizes reflector efficiency at the measurement angle, unless special measures are used to shift that data to a different elevation "rigging" angle. For DSS 43, the holography data were not shifted, and the measurement angle was 34 degrees. Had the holography measurement been carried out at 45 degrees and panels reset to optimize efficiency at that elevation angle, one would expect a rightward shift of the experimental curve in Fig. 9. This would improve the already good fit to the 1.8-mm theoretical curve seen in the figure.

The agreement between theoretical expectations and the DSS 63 and DSS 43 measurements is judged to be excellent.

[2]M. P. Godwin, et al., "Final Report on S-Band Holographic Tests on DSS-43 64 Metre Antenna," Report No. A079, Job No. 50/041, Eikontech Limited, Sheffield, England, September 1985.

Acknowledgment

The author wishes to thank the engineers at the Canberra DSCC, in particular G. Baines, A. Bailey, and R. Livermore, for their efforts in obtaining the data needed for this article. D. Bathker and K. Bartos at JPL provided many useful suggestions for additional analysis, especially regarding the comparison of PO, GTD, and experimental data.

References

[1] S. D. Slobin, "DSS 63 64-meter antenna S- and X-band efficiency and system noise temperature calibration," *TDA Progress Report 42-90* (this issue), vol. Apr.–June 1987, Jet Propulsion Laboratory, Pasadena, Calif., August 15, 1987.

[2] J. A. Turegano and M. J. Klein, "Calibration radio sources for radio astronomy: Precision flux density measurements at 8420 MHz," *Astronomy and Astrophysics*, vol. 86, pp. 46–49, 1980.

Table 1. Adjustments to 100-percent area efficiency for calibration radio sources, DSS 43 64-m calibration, January 1987

Frequency	Radio Source	Adjustment Factor
S-Band (2285 MHz)	3C274	1.000
	3C218	0.975
	0521-365	1.01
X-Band (8420 MHz)	3C274	1.000
	3C218	0.98
	0521-365	0.86

Note: Source 0521-365 is not a DSN standard calibrator, and thus a large adjustment is not unexpected.

Table 2. Coefficients of second-order curve fits for antenna area efficiencies

Efficiency $= a_0 + a_1\theta + a_2\theta^2$
where θ = elevation angle, degrees

Coefficient/Parameter	S-Band (2285 MHz)	X-Band (8420 MHz)
	With Atmosphere (cf. Fig. 1)	With Atmosphere (cf. Fig. 3)
a_0	0.547454	0.3945515
a_1	8.882707E-04	2.388105E-03
a_2	−7.774209E-06	−2.639022E-05
Peak efficiency	0.57283	0.44858
Peak angle, deg	57.129	45.246
Standard deviation	0.00357	0.00506
	Without Atmosphere (cf. Fig. 2)	Without Atmosphere (cf. Fig. 4)
a_0	0.5705453	0.4185152
a_1	2.678935E-04	1.722039E-03
a_2	−2.833061E-06	−2.079413E-05
Peak efficiency	0.57688	0.45417
Peak angle, deg	47.280	41.407
Standard deviation	0.00359	0.00506

Table 3. Coefficients of fourth-order curve fits for S- and X-band system noise temperatures

$$T_{system} = a_0 + a_1\theta + a_2\theta^2 + a_3\theta^3 + a_4\theta^4$$

where θ = elevation angle, degrees

Coefficient/Parameter	S-Band (2285 MHz)[a]	X-Band (8420 MHz)[b]
	With Atmosphere (cf. Fig. 5)	With Atmosphere (cf. Fig. 7)
a_0	5.666247E+01	7.358913E+01
a_1	−2.363757E+00	−3.812552E+00
a_2	6.504466E−02	1.105952E−01
a_3	−8.282610E−04	−1.436480E−03
a_4	3.928624E−06	6.909606E−06
	Note: If $\theta \geq 75°$, T_{system} = 20.138 K	Note: If $\theta \geq 70°$, T_{system} = 21.814 K
Zenith noise temperature	20.138 K	21.814 K
Standard deviation	0.934 K	0.377 K
	Without Atmosphere (cf. Fig. 6)	Without Atmosphere (cf. Fig. 8)
a_0	3.770463E+01	4.703577E+01
a_1	−1.226025E+00	−2.124297E+00
a_2	3.422649E−02	6.186806E−02
a_3	−4.503180E−04	−7.958403E−04
a_4	2.211606E−06	3.778312E−06
	Note: If $\theta \geq 70°$, T_{system} = 18.234 K	Note: If $\theta \geq 70°$, T_{system} = 19.233 K
Zenith noise temperature	18.234 K	19.233 K
Standard deviation	0.905 K	0.313 K

[a]S-band (2285 MHz) specifications: Maser S-TWM1; Block IV; RCP; S/N 4004; 3.01-K noise temperature.

[b]X-band (8420 MHz) specifications: Maser X-TWM2; Block IIA; RCP; S/N 2010; 3.61-K noise temperature.

Table 4. Design expectation for 64-m antenna with dual hybrid mode feedhorn at 8420 MHz and 45-degree elevation angle using physical optics analysis.

Item	Loss, dB	Net Gain, dBi
1. 100% Area Efficiency		75.04
2. Illumination Amplitude	−0.454	
3. Illumination Phase	−0.146	
4. Forward and Rear Spillover	−0.210	
5. Subreflector Blockage	−0.170	
6. $m \neq 1$ modes	−0.035	
7. Cross polarization	−0.0004	74.02
8. Waveguide loss	−0.070	
9. Dichroic plate loss	−0.035	
10. VSWR	−0.039	
11. Quadripod Blockage	−0.677	
12. Main reflector panels		
Manufacturing (0.035 inches)	−0.430	
Setting (0.019 inches)	−0.127	
13. Subreflector		
Manufacturing (0.012 inches)	−0.051	72.59 (= 0.569 efficiency)

Note: The rms panel and subreflector tolerance = 0.04159 in. (1.06 mm)

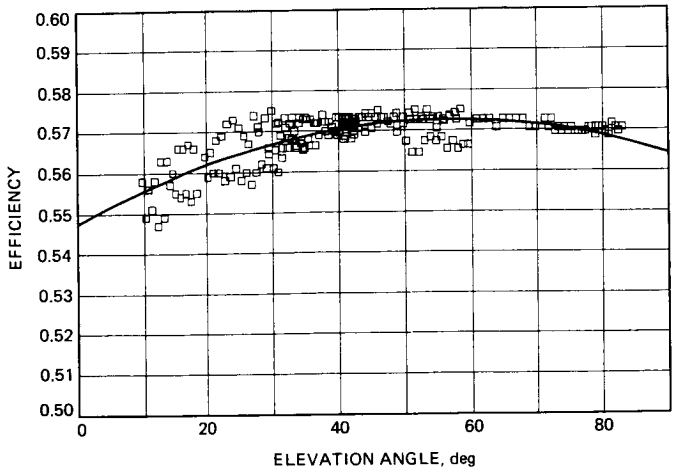

Fig. 1. DSS 43 64-m S-band (2285-MHz) area efficiency with atmospheric attenuation included

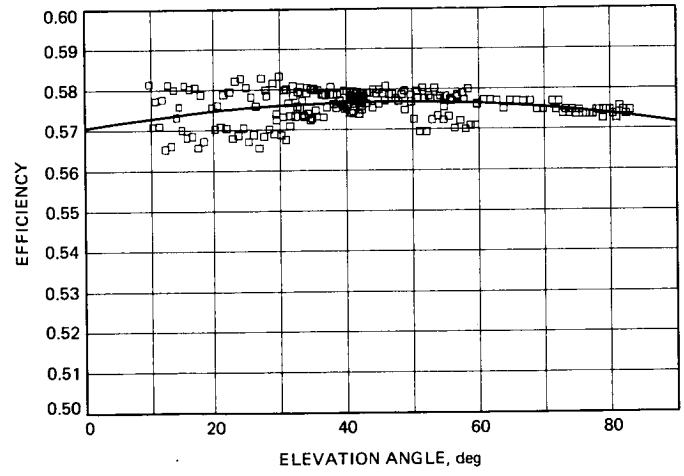

Fig. 2. DSS 43 64-m S-band (2285-MHz) area efficiency without atmospheric attenuation

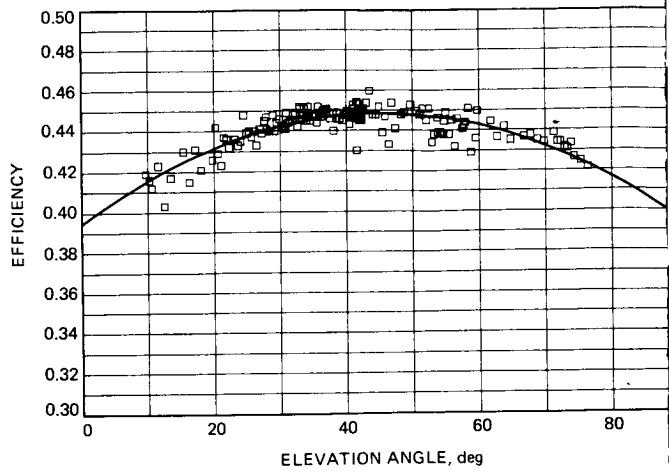

Fig. 3. DSS 43 64-m X-band (8420-MHz) area efficiency with atmospheric attenuation included

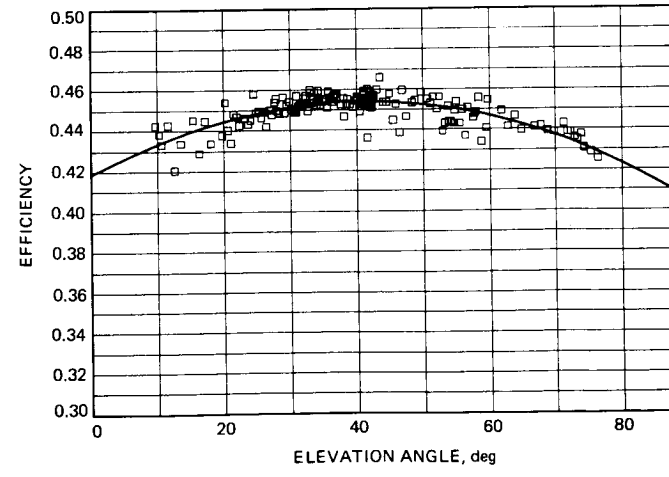

Fig. 4. DSS 43 64-m X-band (8420-MHz) area efficiency without atmospheric attenuation

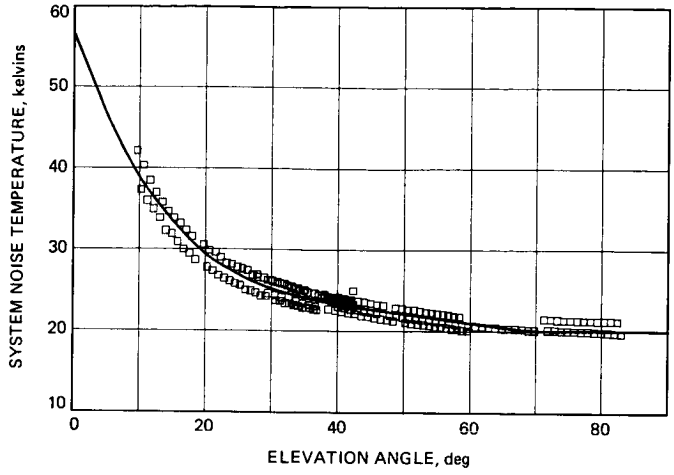

Fig. 5. DSS 43 64-m S-band (2285-MHz) system noise temperature, including atmospheric contribution

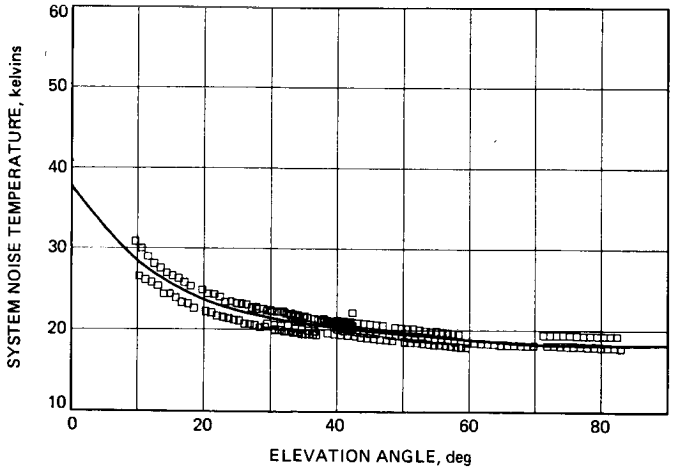

Fig. 6. DSS 43 64-m S-Band (2285-MHz) system noise temperature, without atmospheric contribution

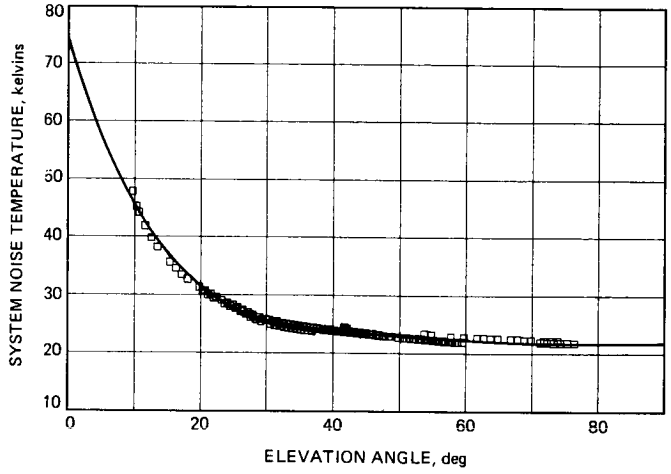

Fig. 7. DSS 43 64-m X-band (8420-MHz) system noise temperature, including atmospheric contribution

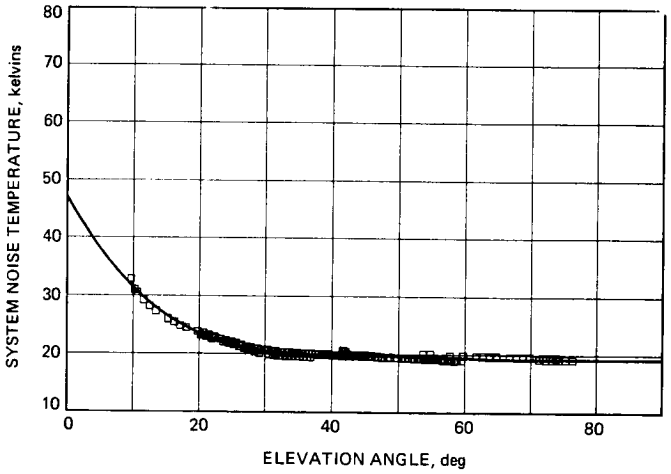

Fig. 8. DSS 43 64-m X-band (8420-MHz) system noise temperature, without atmospheric contribution

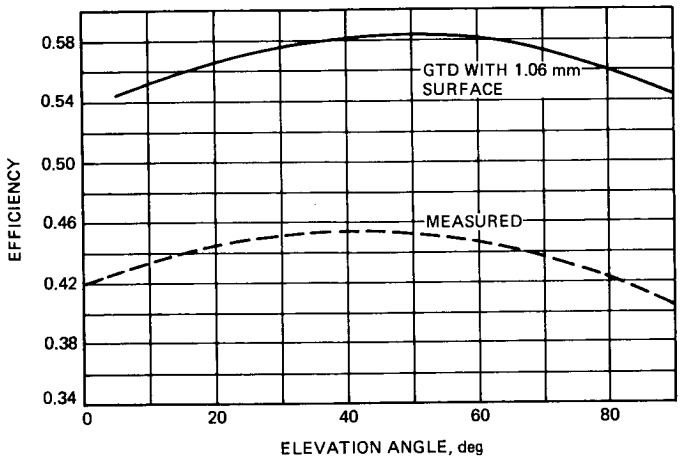

Fig. 9. Comparison of DSS 43 64-m GTD-calculated efficiency (with 1.06-mm rms Ruze surface tolerance) and measured efficiency

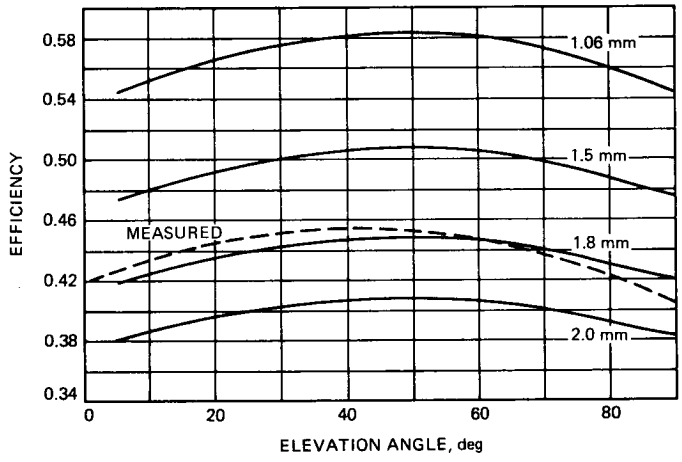

Fig. 10. Comparison of DSS 43 64-m GTD-calculated efficiency and measured efficiency for various Ruze surface tolerance values